

## STRUCTURAL PARAMETERS OF SEVEN SMC INTERMEDIATE-AGE AND OLD STAR CLUSTERS \*

KATHARINA GLATT<sup>1,2</sup>, EVA K. GREBEL<sup>1,2</sup>, JOHN S. GALLAGHER III.<sup>3</sup>, ANTONELLA NOTA<sup>4</sup>, ELENA SABBI<sup>4</sup>, MARCO SIRIANNI<sup>4</sup>, GISELLA CLEMENTINI<sup>5</sup>, GARY DA COSTA<sup>6</sup>, MONICA TOSI<sup>5</sup>, DANIEL HARBECK<sup>3</sup>, ANDREAS KOCH<sup>7</sup>, AND ANDREA KAYSER<sup>1</sup>

*Accepted for publication in AJ*

### ABSTRACT

We present structural parameters for the seven intermediate-age and old star clusters NGC 121, Lindsay 1, Kron 3, NGC 339, NGC 416, Lindsay 38, and NGC 419 in the Small Magellanic Cloud. We fit King profiles and Elson, Fall, and Freeman (EFF) profiles to both surface-brightness and star count data taken with the Advanced Camera for Surveys aboard the Hubble Space Telescope. Clusters older than  $\sim 1$  Gyr show a spread in cluster core radii that increases with age, while the youngest clusters have relatively compact cores. No evidence for post core collapse clusters was found. We find no correlation between core radius and distance from the SMC center, although consistent with other studies of dwarf galaxies, some relatively old and massive clusters have low densities. The oldest SMC star cluster, the only globular NGC121, is the most elliptical object of the studied clusters. No correlation is seen between ellipticity and distance from the SMC center. The structures of these massive intermediate-age (1-8 Gyr) SMC star clusters thus appear to primarily result from internal evolutionary processes.

*Subject headings:* galaxies: star clusters, – galaxies: Magellanic Clouds

### 1. INTRODUCTION

The Small Magellanic Cloud (SMC) contains populous star clusters similar to those found in the Large Magellanic Cloud (LMC), although the two galaxies experienced a very different cluster formation history and age-metallicity relation (e.g., Da Costa 2002). The smaller and less massive SMC contains many fewer clusters than the LMC. It formed its clusters continuously to the present day over the last  $\sim 7.5$  Gyr (age of Lindsay 1, Glatt et al. 2008a). The oldest and only SMC globular star cluster, NGC 121, is 2-3 Gyr younger than the oldest Milky Way (MW) and LMC globular clusters (Glatt et al. 2008b).

Galactic globular clusters (GCs) can be described as an isothermal central region and a tidally truncated outer region (e.g., Binney & Merrifield 1998), but both regions evolve with time. Once formed, star clusters are affected by internal and external processes, which influence the spatial distribution of member stars. The

evolution of star clusters is affected by mass loss caused by, e.g., expulsion of gas, large-scale mass segregation, stellar mass loss, and low-mass star evaporation (e.g., Gnedin & Ostriker 1997; Koch et al. 2004; Lamers et al. 2005; Goodwin & Bastian 2006). The galactic environment causes external perturbations such as tidal shocking that occurs as star clusters cross the disk or pass near the bulge (e.g., Gnedin & Ostriker 1997). These processes tend to decrease the cluster mass and might lead to core collapse, which has been observed in the oldest MW and LMC clusters (Djorgovski & Meylan 1994; Mackey & Gilmore 2003a). The investigation of the present-day structure of individual star clusters is an important instrument to probe cluster dynamical evolution.

In the SMC and the LMC, some of the older objects have apparently experienced a significant change in core radius, while for other old objects the core radii apparently have remained almost unchanged (Mackey & Gilmore 2003a,b). This former trend seems most likely to be the result of real physical cluster evolution, but the processes causing this core expansion for some clusters are not yet understood. A spread in core radii beginning at a few 100 Myr is visible with a few clusters showing large core radii while others remain small and compact. The five Fornax and four confirmed Sagittarius clusters show the same spread: two of the Sagittarius and two of the Fornax clusters have large core radii, while the others have compact cores (Mackey & Gilmore 2003c). Galactic GCs show a spread in core radius size amounting to about two orders of magnitude (Trager et al. 1995) including a large number of so called core-collapse clusters. However, many of the oldest GCs modified their original structure during their lifetime and have developed small cores (e.g., Trager et al. 1995; Bonatto & Bica 2008).

The ellipticity of the SMC clusters was noted to be larger than that of the MW and LMC clus-

\* Based on observations made with the NASA/ESA Hubble Space Telescope, obtained at the Space Telescope Science Institute, which is operated by the Association of Universities for Research in Astronomy, Inc., under NASA contract NAS 5-26555. These observations are associated with program GO-10396.

<sup>1</sup> Department of Physics, University of Basel, Klingelbergstrasse 82, CH-4056 Basel, Switzerland

<sup>2</sup> Astronomisches Rechen-Institut, Zentrum für Astronomie der Universität Heidelberg, Mönchhofstr. 12-14, D-69120 Heidelberg, Germany

<sup>3</sup> Department of Astronomy, University of Wisconsin, 475 North Charter Street, Madison, WI 53706-1582

<sup>4</sup> Space Telescope Science Institute, 3700 San Martin Drive, Baltimore, MD 21218

<sup>5</sup> INAF - Osservatorio Astronomico di Bologna, Via Ranzani 1, 40127 Bologna, Italy

<sup>6</sup> Research School of Astronomy & Astrophysics, The Australian National University, Mt Stromlo Observatory, via Cotter Rd, Weston, ACT 2611, Australia

<sup>7</sup> Department of Physics and Astronomy, University of Leicester, University Road, Leicester, LE1 7RH, UK

ters (Kontizas et al. 1990; Han & Ryden 1994; Goodwin 1997). Old Galactic GCs have a very spherical shape, while the oldest LMC globulars are flatter. The oldest SMC clusters are even flatter than those in the LMC (Kontizas et al. 1990).

If one assumes that star clusters had originally small core regions and elliptical shapes then why was this original structure of many of the Magellanic Cloud (MC) GCs modified during their lifetime and why did some of the oldest clusters hosted by LMC and SMC remain unchanged? Goodwin (1997) proposes that the strength of the tidal field of the parent galaxy is the dominant factor. If the tidal field is strong, the velocity anisotropies in a rapidly rotating elliptical globular cluster are destroyed, while a weak field is unable to remove these anisotropies and the cluster remains unchanged. In the MW, however, one has to distinguish between halo-, bulge-, and disk GCs. Disk GCs move in circular orbits around the MW center and experience only little variation of the Galactic gravitational field. Halo clusters pass the Galactic disk or bulge (Hunter et al. 2003; Lamers et al. 2005; Gieles et al. 2007), which has a strong influence on their dynamical evolution and hence structure. The GC system of the MW also contains a number of clusters acquired via merger processes (e.g., Bica et al. 2006).

We determine the structural parameters of the seven rich SMC star clusters NGC 121, Lindsay 1, Kron 3, NGC 339, NGC 416, Lindsay 38, and NGC 419 by fitting *both* King and EFF profiles to projected number-density and surface-brightness profiles. The observations were obtained with the Advanced Camera for Surveys (ACS) aboard the Hubble Space Telescope (HST). The important characteristic radii of star clusters that we determine are the core radius ( $r_c$ ), the projected half light radius ( $r_h$ ), and the tidal radius ( $r_t$ ). The core radius is defined as the radius at which the surface brightness has fallen to half its central value. The scale radius in the King (1962) analytic profile,  $r_0$ , however exceeds the core radius such that it is larger for lower central concentrations. The difference between  $r_c$  and  $r_0$  is greatest at low concentrations. The half light radius contains half the light of the cluster. The mean SMC distance modulus is assumed to be  $(m - M)_0 = 18.88 \pm 0.1$  mag (60 kpc) (e.g., Storm et al. 2004), but our photometry also provides us with individual cluster distances (Glatt et al. 2008a, Paper I).

Generally, beyond the tidal radius the external gravitational fields of the galaxy dominate the internal dynamics, and stars are no longer bound to the cluster (e.g., Elson et al. 1987; Gnedin & Ostriker 1997). In the MCs it is not obvious that the tidal field has set the observed tidal radii of star clusters. For example Elson et al. (1987) found that ten LMC star clusters with ages up to  $8 \times 10^8$  yrs do not appear to be tidally truncated. This could result, for example, from interactions with other star clusters (Carvalho et al. 2008). Therefore, we use 'limiting radius' for the King model parameter  $r_t$  because it may well be that the limiting radii are not tidally generated.

In § 2 we give an overview of the data and the reduction process, which has been described in detail in Paper I and in Glatt et al. (2008b) (Paper II). The methods used in the present paper are described in § 3 and the results are

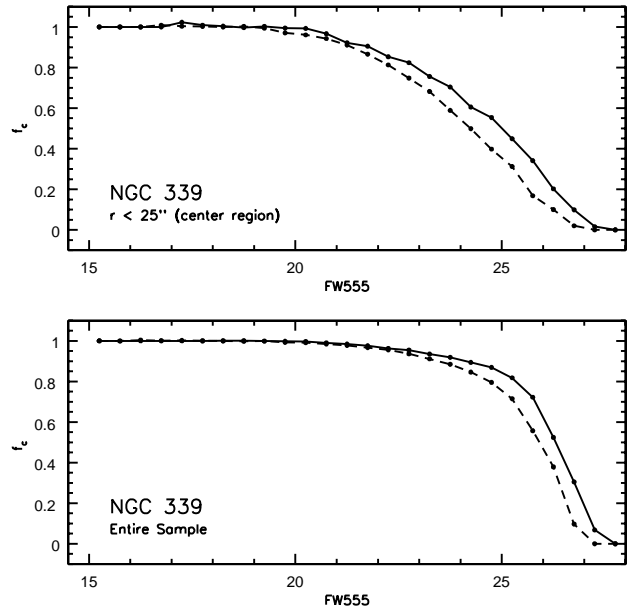


FIG. 1.— Completeness curves for the F555W (solid line) and F814W (dashed line) photometry of NGC 339 as a function of magnitude. The upper plot shows the completeness curves for the center region ( $r < 25''$ ) of the cluster and the lower plot shows the completeness curves for the entire sample. Only stars for which the completeness in the center region is better than 50% in the central regions of each cluster were used.

discussed in § 4.

## 2. OBSERVATIONS

The SMC star clusters NGC 121, Lindsay 1, Kron 3, NGC 339, NGC 416, Lindsay 38, and NGC 419 were observed with the HST/ACS between 2005 August and 2006 March (Table 1 in Paper I). The images were taken in the F555W and F814W filters, which closely resemble the Johnson V and I filters in their photometric properties (Sirianni et al. 2005). All clusters were observed with the Wide Field Channel (WFC), while for the dense central regions of NGC 121, NGC 416, and NGC 419 images from the High Resolution Camera (HRC) are available. Each WFC image covers an area of  $200'' \times 200''$  at each pointing with a pixel scale of  $\sim 0.05$  arcsec. The HRC images cover an area of  $29'' \times 26''$  with a pixel scale of  $\sim 0.025$  arcsec.

The data sets were processed adopting the standard Space Telescope Science Institute ACS calibration pipeline (CALACS) to subtract the bias level and to apply the flat field correction. For each filter, the short and long exposures were co-added independently using the MULTIDRIZZLE package (Koekemoer et al. 2002). Cosmic rays and hot pixels were removed with this package and a correction for geometrical distortion was provided. The resulting data consist of one 40 s and one 1984 s exposure (1940 s for Lindsay 38) in F555W and one 20 s as well as one 1896 s exposure (1852 s for Lindsay 38) in F814W. The HRC data of NGC 419 consist of a 70 s and 1200 s exposure in F555W and a 40 s and 1036 s exposure in F814W.

Saturated foreground stars and background galaxies were discarded from the WFC images by using the Source Extractor (Bertin & Arnouts 1996). The detec-

tion thresholds were set at  $3\sigma$  above the local background level for Lindsay 1,  $1\sigma$  for Kron3 and  $4\sigma$  for NGC 339, NGC 416, and Lindsay 38 in order to detect even the faintest sources. The threshold levels were chosen based on the different crowding effects of the individual clusters. The photometric reductions were carried out using the DAOPHOT package in the IRAF<sup>9</sup> environment on DRIZZLED images. The exposure times, the selection cuts, and the photometry are described in the Papers I and II and we refer to these two papers for detailed information.

### 3. STRUCTURAL PARAMETERS

#### 3.1. Centers

To study the structural parameters of the clusters we first determined the photo-center ( $C_{phot}$ ) of the stellar populations; for a symmetric system this will be close to the center of gravity. An accurate determination of the cluster center is necessary in order to avoid artificial distortions of the radial profiles. As a first approximation we estimated the location of the cluster center on the image by eye. A more precise center was then determined by calculating the average of the x and y coordinates within the cluster center region. First, the mean x and y coordinates were determined within a radius of 2000 pixels around the apparent center. In the following iterations, the radii were divided by two using the center coordinates found in the previous iterations as their origin. We iterated until the radius was smaller than 10 pixels. The error is  $\sim 0.5''$  for both  $\alpha$  and  $\delta$ , which corresponds to 10 pixels in the HST/ACS images. For NGC 121, NGC 416, and NGC 419  $C_{phot}$  was determined on the HRC data using the same algorithm due to crowding of the WFC data. The resulting positions are summarized in Table 1.

#### 3.2. King profile

The number surface density profiles of old GCs are usually described by the empirical King models (King 1962):

$$n(r) = k \cdot \left\{ \frac{1}{[1 + (r/r_0)^2]^{1/2}} - \frac{1}{[1 + (r_t/r_0)^2]^{1/2}} \right\}^2 + \phi, \quad (1)$$

where  $n(r)$  is the number of stars per unit area,  $r_0$  is the King radius, and  $r_t$  is the limiting radius of the cluster. The parameter  $\phi$  was added for the background contamination. No adjacent field was observed to measure the background. The field-of-view of ACS is too small for a reliable measurement of the background on the image. As a result we cannot necessarily distinguish an extended halo around a cluster from the true stellar background. Hence, we treat  $\phi$  as a fitting parameter and assume that the background density  $\phi$  is constant for each cluster. Although our background estimates are formally quite good, our values of  $\phi$  can be considered as being greater than or equal to the actual background. Both for the number density and surface-brightness dis-

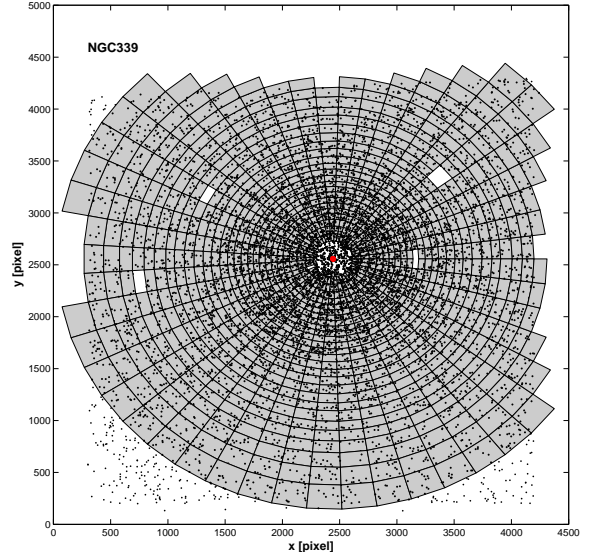


FIG. 2.— Star selection to calculate the number density profiles for NGC 339 as this is representative for all clusters. Those stars lying within the gray area were counted while the grey areas represent the parts of the annuli in which these stars are found. The red dot indicates the location of the center of gravity.

tributions King profiles were fitted, which are summarized in Table 2 (upper and middle sections).

Due to the field-of-view of the WFC the limiting radii of our clusters lie outside the ACS image. Therefore, the limiting radius  $r_t$  and as a consequence also the half-light radius  $r_h$  cannot be directly measured. We give an estimate of the projected half-light radius  $r_h$  by calculating the total luminosity from the King profiles. The values  $r_0$  and  $r_t$  can be used to calculate the concentration parameter  $c = \log(r_t/r_0)$ . From  $r_h$  we can give an estimate of the absolute magnitude  $M_V$  of the star clusters by multiplying the flux within  $r_h$  by 2. Using the distance moduli and the extinctions from Paper I,  $M_V$  can be calculated. The result is summarized in Table 3.

Concentric annuli containing the same number of stars were constructed around  $C_{phot}$ . The radii and the enclosed number of stars depend on the richness of the clusters and on photometric incompleteness caused by crowding. The completeness corrections on the WFC images were determined for each cluster separately and applied to the number density calculation. The completeness factors were determined using the subroutine *addstar* in DAOPHOT to simulate 1,000,000 artificial stars (in steps of  $\approx 2500$  stars) in each long exposure frame. For a detailed description of the procedure we refer the reader to Sabbi et al. (2007). Figure 1 shows the completeness factor of NGC 339 in each filter, defined as the percentage of the artificial stars successfully recovered compared with the total number of stars added to the data. Only stars brighter than the magnitude for which the completeness is 50% in the central regions of each cluster were used.

Then the area of the annuli was calculated. We had to apply a geometrical area correction for those annuli that were not fully imaged due to the cluster centering in the upper right part of the MULTIDRIZZLED image. Therefore, only those parts of the annuli were considered

<sup>9</sup> IRAF is distributed by the National Optical Astronomy Observatory, which is operated by the Association of Universities for Research in Astronomy, Inc. under cooperative agreement with the National Science Foundation.

TABLE 1  
POSITION OF THE PHOTO-CENTER

Cluster	$\alpha$	$\delta$	$[Fe/H]_{ZW84}$	age Gyr	distance kpc
NGC 121	$0^h 26^m 47^s .80$	$-71^\circ 32' 11'' .40$	$-1.46 \pm 0.10$	$10.5 \pm 0.5$	$64.9 \pm 1.2$
Lindsay 1	$0^h 03^m 53^s .22$	$-73^\circ 28' 16'' .66$	$-1.14 \pm 0.10$	$7.5 \pm 0.5$	$56.9 \pm 1.0$
Kron 3	$0^h 24^m 46^s .28$	$-72^\circ 47' 35'' .76$	$-1.08 \pm 0.12$	$6.5 \pm 0.5$	$60.6 \pm 1.1$
NGC 339	$0^h 57^m 46^s .38$	$-74^\circ 28' 14'' .24$	$-1.12 \pm 0.10$	$6 \pm 0.5$	$57.6 \pm 4.1$
NGC 416	$1^h 07^m 58^s .64$	$-72^\circ 21' 19'' .75$	$-1.00 \pm 0.13$	$6 \pm 0.8$	$60.4 \pm 1.9$
Lindsay 38	$0^h 48^m 50^s .03$	$-69^\circ 52' 07'' .63$	$-1.59 \pm 0.10$	$6.5 \pm 0.5$	$66.7 \pm 1.6$
NGC 419	$1^h 08^m 17^s .31$	$-72^\circ 53' 02'' .49$	$-0.67 \pm 0.12$	1.2-1.6	$50.2 \pm 2.6$

<sup>a</sup>The values for the metallicities [Fe/H] are adopted from Da Costa & Hatzidimitriou (1998) and Kayser et al. 2010, in prep. The ages are taken from Paper I and II (best-fitting Dartmouth isochrones (Dotter et al. 2007) for all clusters except NGC 419, for which the Padova isochrones (Girardi et al. 2000, 2008) provided the best fit.)

TABLE 2  
STRUCTURAL PARAMETERS FROM THE KING PROFILE FIT

Cluster	$r_0$ arcsec	$r_0^1$ pc	$r_t$ arcsec	$r_t^1$ pc	c	$r_h$ arcsec	$r_h$ pc	$\phi$
<i>To number-density profiles</i>								
NGC 121	$15.26 \pm 0.42$	$4.80 \pm 0.56$	$165.01 \pm 23.28$	$51.92 \pm 7.32$	$1.034 \pm 0.12$	$27.01 \pm 2.21$	$8.50 \pm 0.70$	$10^{-3}$
Lindsay 1	$61.67 \pm 3.80$	$17.01 \pm 1.55$	$230.77 \pm 37.26$	$63.66 \pm 10.28$	$0.573 \pm 0.10$	$62.45 \pm 5.84$	$17.23 \pm 1.61$	$10^{-5}$
Kron 3	$34.86 \pm 1.07$	$10.24 \pm 0.87$	$130.96 \pm 6.70$	$38.47 \pm 1.97$	$0.575 \pm 0.02$	$35.38 \pm 1.50$	$10.39 \pm 0.44$	$10^{-2}$
NGC 339	$32.84 \pm 0.64$	$9.17 \pm 0.75$	$186.73 \pm 16.51$	$52.14 \pm 5.10$	$0.755 \pm 0.06$	$41.85 \pm 2.37$	$11.69 \pm 0.66$	$10^{-2}$
NGC 416	$11.76 \pm 0.95$	$3.44 \pm 0.44$	$84.59 \pm 19.65$	$24.77 \pm 5.75$	$0.859 \pm 0.16$	$16.96 \pm 2.63$	$4.97 \pm 0.77$	$10^{-2}$
Lindsay 38	$31.24 \pm 0.85$	$10.10 \pm 0.84$	$173.82 \pm 12.39$	$56.21 \pm 4.00$	$0.745 \pm 0.04$	$39.40 \pm 1.65$	$12.74 \pm 0.53$	$10^{-2}$
NGC 419	$15.22 \pm 1.78$	$3.70 \pm 0.51$	$174.15 \pm 18.57$	$42.38 \pm 4.52$	$1.059 \pm 0.08$	$27.69 \pm 2.47$	$6.74 \pm 0.60$	$10^{-2}$
<i>To surface-brightness profiles</i>								
NGC 121	$11.56 \pm 0.98$	$3.64 \pm 0.31$	$175.52 \pm 33.19$	$55.22 \pm 10.44$	$1.246 \pm 0.16$	$24.15 \pm 3.20$	$7.60 \pm 1.00$	$10^{-5}$
Lindsay 1	$61.41 \pm 4.95$	$16.94 \pm 1.37$	$216.54 \pm 41.92$	$59.73 \pm 11.57$	$0.349 \pm 0.08$	$60.08 \pm 8.62$	$16.57 \pm 2.37$	$10^{-5}$
Kron 3	$25.53 \pm 2.41$	$7.50 \pm 0.71$	$180.25 \pm 37.56$	$52.96 \pm 11.03$	$0.848 \pm 0.15$	$36.50 \pm 3.50$	$10.72 \pm 1.03$	$10^{-5}$
NGC 339	$35.29 \pm 2.86$	$9.86 \pm 0.80$	$260.72 \pm 39.79$	$72.80 \pm 11.11$	$0.869 \pm 0.14$	$51.58 \pm 5.89$	$14.40 \pm 1.65$	$10^{-5}$
NGC 416	$10.22 \pm 1.51$	$2.99 \pm 0.44$	$107.95 \pm 22.54$	$31.61 \pm 6.60$	$1.023 \pm 0.15$	$17.88 \pm 3.18$	$5.24 \pm 0.93$	$10^{-2}$
Lindsay 38	$31.47 \pm 3.68$	$10.18 \pm 1.19$	$179.65 \pm 34.08$	$58.09 \pm 11.02$	$0.711 \pm 0.05$	$40.32 \pm 6.13$	$13.04 \pm 1.98$	$10^{-5}$
NGC 419	$12.98 \pm 1.47$	$3.16 \pm 0.36$	$207.19 \pm 30.11$	$50.42 \pm 7.33$	$1.203 \pm 0.15$	$27.73 \pm 3.58$	$6.75 \pm 0.87$	$10^{-5}$
<i>To surface-brightness profiles for stars below the MSTOs</i>								
NGC 121	$26.24 \pm 1.11$	$8.26 \pm 0.35$	$156.25 \pm 28.88$	$49.16 \pm 9.09$	$0.775 \pm 0.11$	$34.31 \pm 3.91$	$10.80 \pm 1.23$	$10^{-2}$
Lindsay 1	$78.21 \pm 4.48$	$21.57 \pm 1.24$	$269.84 \pm 50.11$	$74.44 \pm 13.82$	$0.538 \pm 0.07$	$75.58 \pm 9.83$	$20.85 \pm 2.71$	$10^{-5}$
Kron 3	$30.50 \pm 1.48$	$8.96 \pm 0.44$	$157.86 \pm 30.84$	$46.38 \pm 9.06$	$0.714 \pm 0.08$	$37.01 \pm 4.60$	$10.87 \pm 1.35$	$10^{-2}$
NGC 339	$32.54 \pm 2.05$	$9.09 \pm 0.57$	$271.17 \pm 52.07$	$75.72 \pm 14.55$	$0.921 \pm 0.12$	$50.59 \pm 5.92$	$14.13 \pm 1.65$	$10^{-2}$
NGC 416	$15.10 \pm 0.89$	$4.42 \pm 0.26$	$76.01 \pm 18.66$	$22.26 \pm 5.46$	$0.702 \pm 0.12$	$18.05 \pm 2.81$	$5.29 \pm 0.82$	$10^{-5}$
Lindsay 38	$29.01 \pm 1.84$	$9.38 \pm 0.60$	$192.65 \pm 38.72$	$62.30 \pm 12.52$	$0.822 \pm 0.06$	$40.16 \pm 5.29$	$12.99 \pm 1.71$	$10^{-2}$
NGC 419	$15.60 \pm 1.66$	$3.80 \pm 0.40$	$275.91 \pm 53.94$	$67.15 \pm 13.13$	$1.247 \pm 0.12$	$35.03 \pm 5.18$	$8.53 \pm 1.26$	$10^{-2}$

<sup>1</sup> The MSTOs and the conversion of  $r_0$  is based on the distances found in Paper I. The upper section of this table corresponds to the Figures 3, and 4 (solid lines), the middle section to Figures 5 and 6 (dashed lines) for which only stars brighter than the magnitude for which the completeness is 50% in the central region of each cluster were used. The lower section corresponds to the Figures 8 and 9 (dashed lines) for which only stars brighter than the magnitude for which the completeness is 50% in the central region of each cluster and stars fainter than the MSTOs were used. The half-light radii were computed by estimating  $L_{tot}$  from the King profiles.

TABLE 3  
ESTIMATE OF THE ABSOLUTE MAGNITUDES

Cluster	$(m - M)_0$ mag	$E_{V-I}$ mag	$M_V^{King}$ mag	$M_V^{EFF}$ mag
NGC 121	$19.06 \pm 0.03$	0.024	$-8.51 \pm 0.15$	$-8.37 \pm 0.14$
Lindsay 1	$18.78 \pm 0.04$	0.024	$-7.39 \pm 0.09$	$-7.38 \pm 0.09$
Kron 3	$18.91 \pm 0.04$	0.024	$-7.75 \pm 0.15$	$-8.10 \pm 0.12$
NGC 339	$18.80 \pm 0.08$	0.040	$-7.42 \pm 0.14$	$-7.76 \pm 0.11$
NGC 416	$18.90 \pm 0.07$	0.104	$-8.03 \pm 0.11$	–
Lindsay 38	$19.12 \pm 0.05$	0.016	$-5.08 \pm 0.19$	$-5.49 \pm 0.21$
NGC 419	$18.50 \pm 0.12$	0.080	$-8.85 \pm 0.18$	–

<sup>a</sup>The distance moduli and the reddenings  $E_{V-I}$  are taken from Paper I.

that lie fully on the image while the others were excluded. Figure 2 displays the selected areas and stars of NGC 339 as this is representative for all clusters. The black dots lying within the grey area represent the stars considered in the number density profile, while the filled grey areas show the annuli parts in which these stars were found. The errors were propagated from the Poisson statistics of the number and area counts. For NGC 121, NGC 416, and NGC 419 the profiles were obtained on the WFC and HRC data independently and then combined. The WFC data were only considered outside the HRC field, hence avoiding overlaps.

The star density was obtained by dividing the number of stars by their area. Both the King and the EFF profiles were fitted to each of our clusters via  $\chi^2$  minimization.

In Figure 3 and 4 we show the stellar density distribution of our clusters with the best-fitting King profiles (solid line) and the best-fitting EFF profiles (dashed line) plus background. The filled circles represent the star density taken from the WFC data, the open circles the star density taken from the HRC data. The resulting structural parameters  $r_0, r_t, r_h,$  and  $c$  from the King profiles are summarized in Table 2. The parameters  $r_c, r_t, \gamma,$  and  $\phi$  from the EFF profiles are shown in Table 4. The listed errors are given by the  $\chi^2$  minimization fitting process.

### 3.3. EFF profile

The EFF profile (Elson et al. 1987) is given by

$$n(r) = n_0 \cdot (1 + r^2/a^2)^{-\gamma/2} + \phi, \quad (2)$$

where  $n_0$  is the central projected stellar density,  $a$  is a measure of the core radius and  $\gamma$  is the power-law slope. The parameter  $\phi$  was added for the background contamination. The parameter  $a$  in the EFF profiles is related to the core radius of a cluster by  $r_c = a \cdot (2^{2/\gamma} - 1)^{1/2}$ . To determine the parameters of the clusters we fitted the surface brightness profiles with  $I(r) = I_0 \cdot [(1 + r^2/a^2)^{-\gamma/2}] + \phi$ . No limiting radii can be derived from EFF profiles. We give an estimate of the projected half-light radius  $r_h$  by calculating the total luminosity from the EFF profiles. This method works well until  $\gamma \approx 2$  is reached, because then the total luminosity formally becomes infinite.

The EFF profiles were used in this study, because all recent studies (Kontizas et al. 1982; Kontizas & Kontizas 1983; Kontizas et al. 1986,

1990; Mackey & Gilmore 2003b; Hill & Zaritsky 2006; Carvalho et al. 2008) of structure parameters of SMC star clusters used EFF profiles. This choice facilitates the comparison of our results with the earlier studies. For the same reason we chose to work in the commonly used F555W ( $\sim V$ ) band.

In order to measure the surface-brightness profiles, concentric annuli of coextensive areas were created around  $C_{phot}$ . The surface brightness  $\mu_i$  of the  $i$ th annulus in a set was found by summing over the flux of all stars that fall into the annulus. For NGC 416, the profile was fitted only using the inner points ( $\log(r) < 1.5$  arcsec), because the SMC field contribution is not negligible for this cluster. The same area and completeness corrections as for the number density profiles were applied. Saturated foreground stars were removed from the images. Only stars brighter than the magnitude for which the completeness is 50% in the central region of each cluster were used.

For Lindsay 1, Kron 3, NGC 339, and Lindsay 38 only WFC photometry is available, which resolves the clusters entirely. The surface brightness measured in four sets of concentric annuli with the same area are plotted for each cluster in Figure 5. The first set was done with  $76 \text{ arcsec}^2$  (pentagons, black), the second with  $250 \text{ arcsec}^2$  (triangles, magenta), the third with  $374 \text{ arcsec}^2$  (crosses, blue), and the fourth with  $500 \text{ arcsec}^2$  (squares, red).

For the three densest clusters, NGC 121, NGC 416, and NGC 419, the central regions were observed with HST/HRC. The surface brightness profiles of the center region were determined using the HRC data, while the profiles of the outer regions were calculated using the WFC data. Three HRC sets measured in concentric annuli of the same area are displayed with different symbols (green):  $37.5 \text{ arcsec}^2$  (triangles),  $25 \text{ arcsec}^2$  (asterisks), and  $50 \text{ arcsec}^2$  (circles). For the WFC data, the same areas as above have been used, but only those annuli are shown that lie outside the regions covered by the HRC data. The surface-brightness profiles were fitted via  $\chi^2$  minimization.

Two sets of EFF profiles were fitted. For the first set, all stars brighter than the magnitude for which the completeness is 50% in the central region of each cluster were used. The resulting parameters can be compared with literature values. The best-fitting EFF profiles are shown in Figures 5 and 6 (solid lines). The results are summarized in Table 4 (upper and middle section).

The surface brightness comes mostly from the brighter stars around the main-sequence turnoff (MSTO) and brighter, while the surface density distribution comes principally from the numerous stars below the MSTO. Due to the long 2-body relaxation times, we do not expect much mass segregation and therefore the surface brightness and surface density profiles should be the same. To check this assumption, we fitted a second set of EFF profiles using only stars fainter than the MSTO and brighter than the magnitude for which the completeness is 50% in the cluster central regions. The MSTOs were adopted from Paper I. The best-fitting EFF profiles are shown in Figures 8 and 9 (solid lines). The results are summarized in Table 4 (lower section). The profiles are much less scattered and smoother toward the outer region than in the first set of profiles. The reason

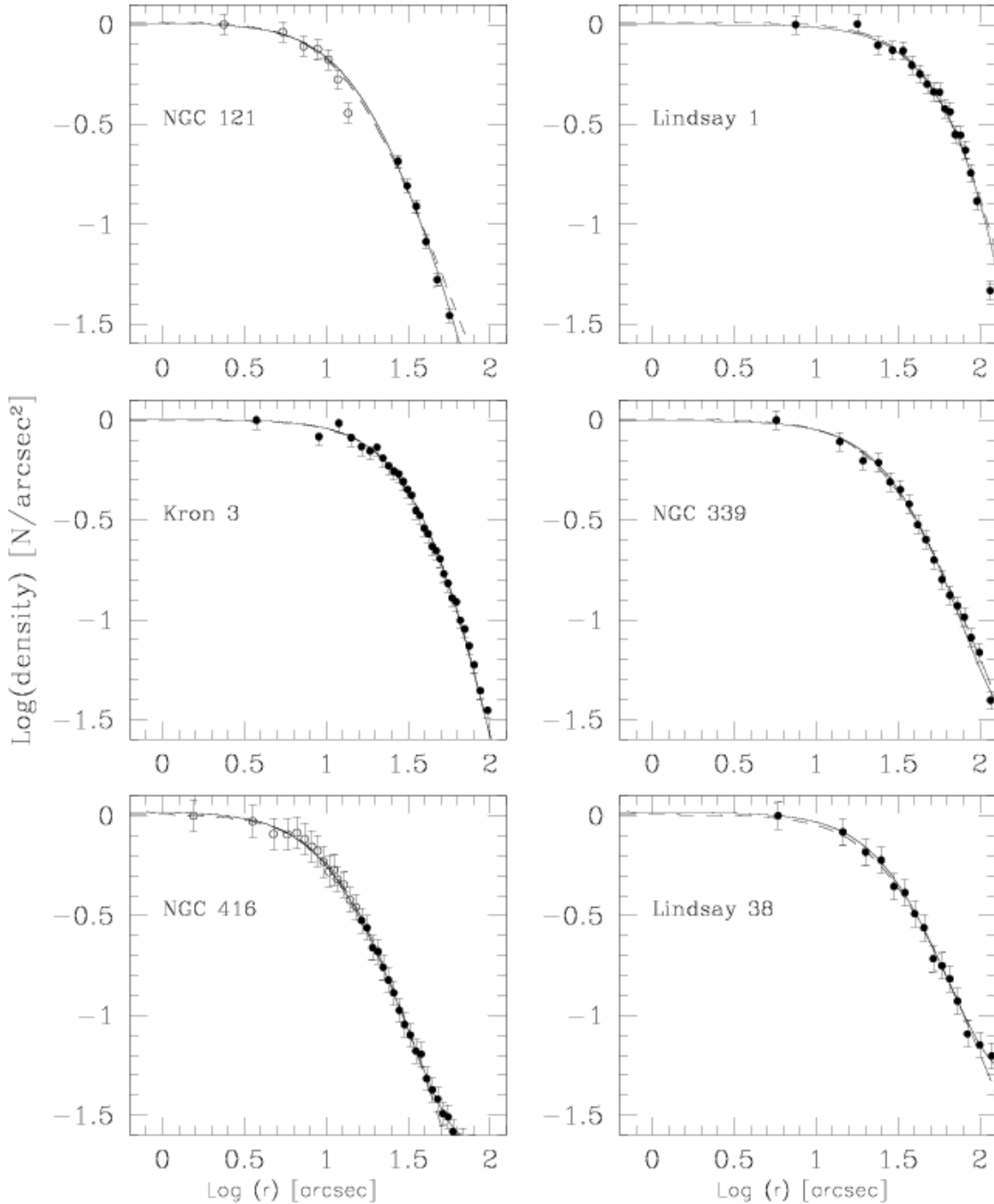


FIG. 3.— Number density profiles of the seven SMC clusters in our sample. The filled circles represent the WFC data, the open circles the HRC data. The solid line indicates the best-fitting King model and the dashed line the best-fitting EFF model of the radial density distribution of the clusters. The radial plots of NGC 416 and NGC 419 (Fig. 4) are truncated.

for the smoother profiles is probably that the number of stars contributing to the surface brightness is larger, and hence statistical fluctuations are smaller.

Cluster core 2-body relaxation times range from 1-2 Gyr on upwards, and thus mass segregation from this process is only expected to be a factor in the densest and oldest clusters in the sample. Only in NGC 121 differences are seen at a possibly significant level in the expected sense of larger core radii for the low mass stars exceeding the combined errors by more than a factor of three. Thus we find no compelling evidence for mass seg-

regation in the seven intermediate mass clusters in our sample, although we emphasize that deeper observations are needed for a definitive test.

Both for the number density and surface-brightness distributions King profiles were fitted, which are summarized in the upper and middle sections of Table 2 for the sample containing all stars above the 50% completeness levels and in the lower section for all stars between the 50% completeness levels and the MSTOs.

TABLE 4  
STRUCTURAL PARAMETERS FROM THE EFF PROFILE FIT

Cluster	$\mu_{555}(0)$ <i>mag/arcsec</i> <sup>2</sup>	a arcsec	$r_c$ arcsec	$r_c^1$ pc	$\gamma$	$r_h$ arcsec	$r_h$ pc	$\phi$
<i>To number-density profiles</i>								
NGC 121	$18.87 \pm 0.03$	$14.63 \pm 2.85$	$13.42 \pm 2.62$	$4.22 \pm 00.82$	2.27	—	—	$10^{-5}$
Lindsay 1	$21.25 \pm 0.04$	$74.84 \pm 32.40$	$48.53 \pm 19.00$	$13.39 \pm 5.24$	3.95	$76.18 \pm 32.98$	$21.01 \pm 9.10$	$10^{-5}$
Kron 3	$20.56 \pm 0.03$	$45.31 \pm 7.89$	$28.66 \pm 4.99$	$8.42 \pm 1.47$	4.12	$43.54 \pm 7.58$	$12.79 \pm 2.23$	$10^{-5}$
NGC 339	$20.03 \pm 0.03$	$29.07 \pm 5.49$	$27.58 \pm 5.21$	$7.70 \pm 1.46$	2.16	—	—	$10^{-5}$
NGC 416	$18.21 \pm 0.06$	$13.73 \pm 2.92$	$11.27 \pm 2.40$	$3.30 \pm 0.70$	2.69	$34.98 \pm 7.42$	$10.22 \pm 2.17$	$10^{-2}$
Lindsay 38	$22.90 \pm 0.04$	$29.07 \pm 9.51$	$27.58 \pm 5.02$	$8.92 \pm 1.62$	2.16	—	—	$10^{-5}$
NGC 419	$18.18 \pm 0.03$	$14.68 \pm 2.67$	$14.20 \pm 2.52$	$3.46 \pm 0.61$	1.05	—	—	$10^{-5}$
<i>To surface-brightness profiles</i>								
NGC 121	$18.60 \pm 0.08$	$16.52 \pm 0.76$	$11.91 \pm 0.57$	$3.75 \pm 0.39$	3.36	$22.66 \pm 0.99$	$7.13 \pm 0.31$	$10^{-5}$
Lindsay 1	$21.94 \pm 0.09$	$101.15 \pm 4.52$	$50.05 \pm 1.96$	$13.81 \pm 0.60$	6.33	$62.14 \pm 1.76$	$17.14 \pm 0.48$	$10^{-5}$
Kron 3	$20.13 \pm 0.09$	$30.11 \pm 1.35$	$22.79 \pm 0.78$	$6.70 \pm 0.26$	3.06	$49.47 \pm 1.41$	$14.53 \pm 0.33$	$10^{-5}$
NGC 339	$21.31 \pm 0.10$	$38.71 \pm 1.52$	$29.02 \pm 1.19$	$8.10 \pm 0.11$	3.11	$61.06 \pm 2.10$	$17.05 \pm 0.45$	$10^{-5}$
NGC 416	$18.31 \pm 0.04$	$9.20 \pm 0.50$	$9.04 \pm 0.35$	$2.65 \pm 0.07$	2.05	—	—	$1.8 \times 10^{-2}$
Lindsay 38	$23.21 \pm 0.06$	$37.83 \pm 1.47$	$28.76 \pm 1.17$	$9.30 \pm 0.48$	3.04	$64.71 \pm 1.84$	$20.93 \pm 0.55$	$10^{-5}$
NGC 419	$17.70 \pm 0.06$	$12.33 \pm 0.56$	$11.73 \pm 0.47$	$2.85 \pm 0.09$	2.15	—	—	$10^{-2}$
<i>To surface-brightness profiles for stars below the MSTOs</i>								
NGC 121	$21.90 \pm 0.07$	$35.59 \pm 0.86$	$23.46 \pm 0.59$	$7.38 \pm 0.21$	3.99	$35.72 \pm 0.86$	$11.24 \pm 0.27$	$10^{-5}$
Lindsay 1	$21.89 \pm 0.10$	$111.84 \pm 3.61$	$64.48 \pm 2.29$	$17.79 \pm 0.63$	5.11	$83.83 \pm 2.70$	$23.13 \pm 0.74$	$10^{-5}$
Kron 3	$21.79 \pm 0.08$	$34.17 \pm 0.17$	$25.31 \pm 0.48$	$7.44 \pm 0.12$	3.20	$50.40 \pm 0.95$	$14.81 \pm 0.28$	$10^{-5}$
NGC 339	$22.37 \pm 0.11$	$29.90 \pm 0.18$	$28.32 \pm 1.35$	$7.91 \pm 0.38$	2.19	—	—	$10^{-5}$
NGC 416	$20.91 \pm 0.06$	$18.91 \pm 0.56$	$17.08 \pm 0.51$	$5.00 \pm 0.16$	2.42	$96.70 \pm 2.86$	$28.32 \pm 0.83$	$1.8 \times 10^{-2}$
Lindsay 38	$24.67 \pm 0.09$	$25.80 \pm 1.88$	$25.20 \pm 1.71$	$8.15 \pm 0.59$	2.07	—	—	$10^{-5}$
NGC 419	$11.62 \pm 0.56$	$14.37 \pm 0.49$	$17.65 \pm 0.58$	$3.50 \pm 0.10$	1.56	—	—	$10^{-2}$

<sup>1</sup> The conversion of  $r_c$  is based on the distances found in Paper I. The upper section of this table corresponds to the Figures 5 and 6 (solid lines), the middle section to the Figures 3 and 4 (dashed lines) for which only stars brighter than the magnitude for which the completeness is 50% in the central region of each cluster were used. The third section of this table corresponds to the Figures 8 and 9 (solid lines) for which only stars brighter than the magnitude for which the completeness is 50% in the central region of each cluster and stars fainter than the MSTOs were used. The half-light radii were computed by estimating  $L_{tot}$  from the EFF profiles. For the clusters with a  $\gamma$  close to two a formally infinite model luminosity was derived and no half-light radius could be calculated.

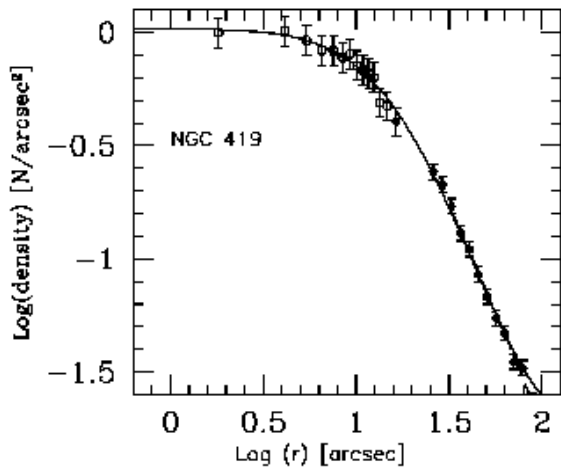


FIG. 4.— As for Fig. 3 but for NGC 419.

### 3.4. Angular distribution and ellipticity

To calculate the projected angular distribution we chose all stars around  $C_{phot}$  that lie entirely inside a circle on the image (see Table 5). Because the clusters are

centered in the upper chip of the camera and the tidal radii lie outside the ACS images, this restriction was necessary to avoid artificial fluctuations. Our cluster samples were subdivided into 12 degree sectors and plotted against the azimuthal angle  $\theta$ . We used a maximum-likelihood approach (McLaughlin et al. 1994, 1995) to obtain a solution for the ellipticity  $\epsilon$ . The observed number density for an intrinsically elliptical distribution of points sampled in *circular* annuli is given by

$$\sigma(R, \theta) = kR^{-\alpha} [\cos^2(\theta - \theta_p) + (1 - \epsilon)^{-2} \sin^2(\theta - \theta_p)]^{-\alpha/2} + \sigma_b \quad (3)$$

where  $\theta_p$  is the position angle of the major axis,  $\sigma_b$  the background density, and the radial falloff is modeled as a simple power law with an exponent  $\alpha$ .

To get a constraint on  $\sigma_b$  we use the distribution of stars in the color-magnitude diagrams (CMDs) of the clusters. Because the SMC is not crowded and because it is located at high Galactic latitude (e.g., Ratnatunga & Bahcall 1985), we do not expect field star contamination levels to be a significant problem. We select those objects directly in the cluster CMDs that are definitely not cluster members (carefully excluding e.g. asymptotic giant branch (AGB) and blue straggler star

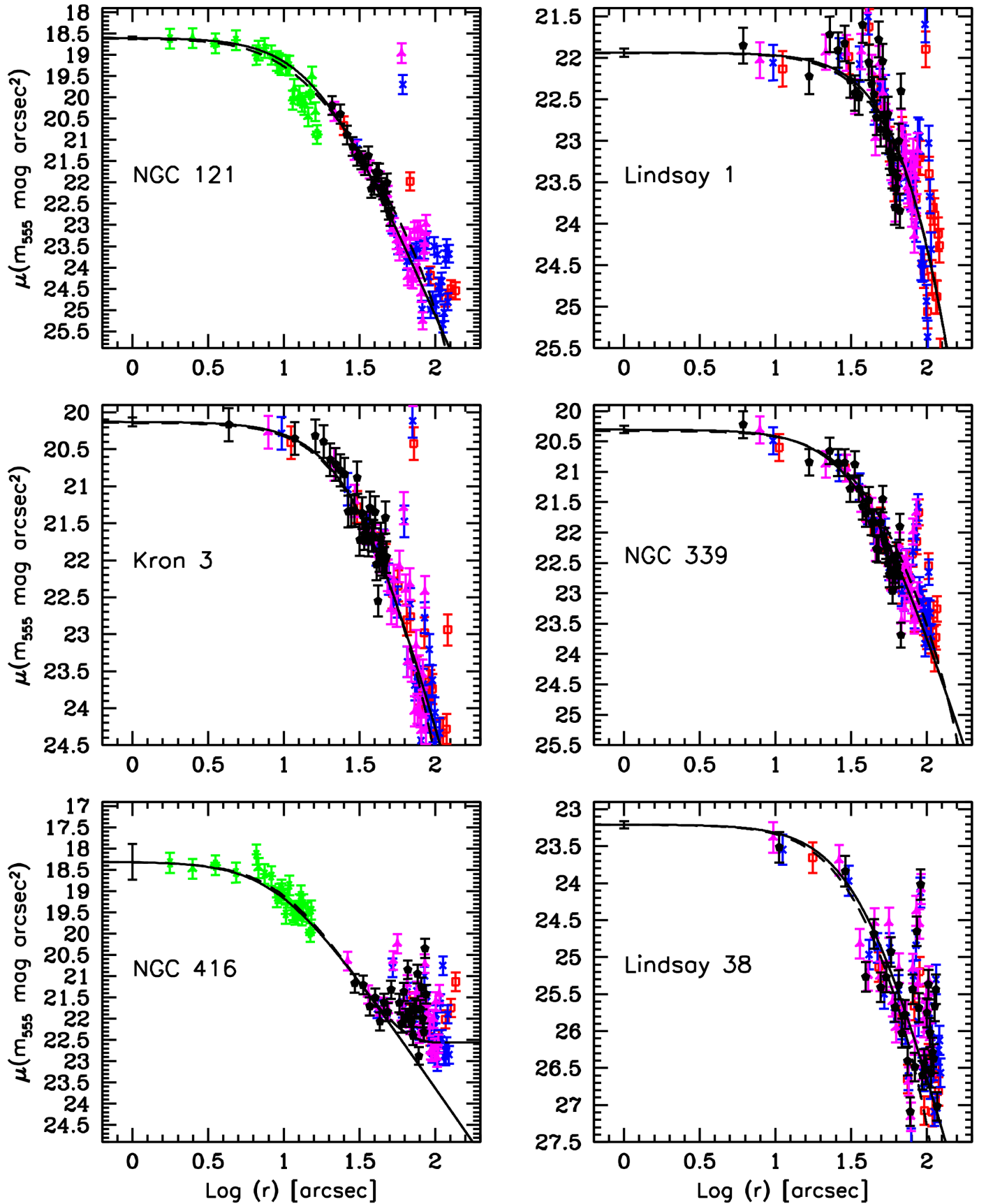


FIG. 5.— Surface-brightness profiles for each of the seven clusters in the present sample in the F555W-band. Only cluster stars brighter than the magnitude for which the completeness is 50% in the central region of each cluster were used. The surface-brightness was measured in four different areas which we display using different symbols (and different colors). For Lindsay 1, Kron 3, NGC 339, and Lindsay 38 only WFC images were used, while for NGC 121, NGC 416, and NGC 419 (Fig. 6) the dense center regions are covered with HRC data. The solid line indicates the best-fitting EFF model and the dashed line the best-fitting King model of the surface-brightness distribution.



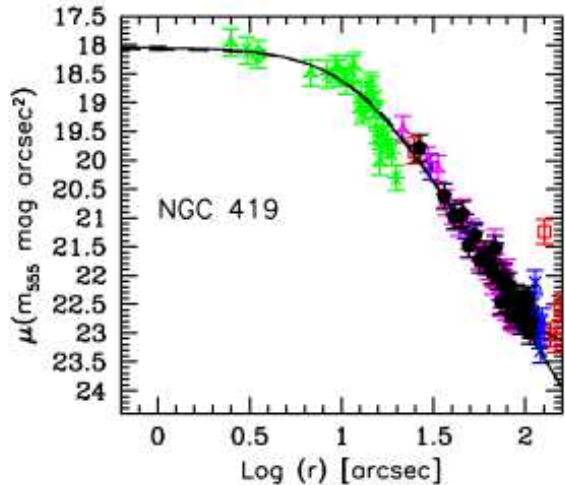
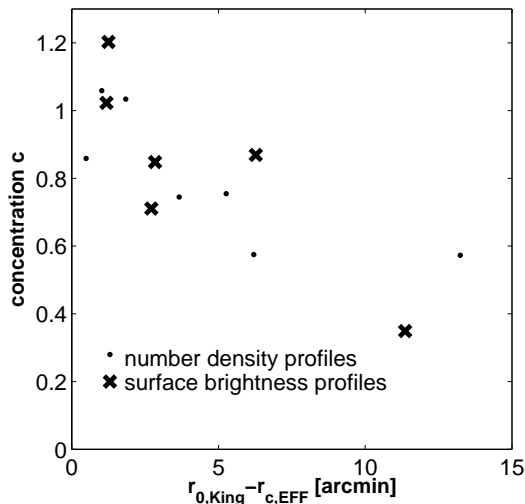


FIG. 6.— As for Fig. 5 but for NGC 419.

FIG. 7.— Difference between the King profile scale radius  $r_0$  and the core radius  $r_c$  from EFF profiles as a function of the concentration parameter  $c$ .

(BSS) stars). We use the number of these objects to estimate the background. The normalized background contaminations  $\sigma_b$  are then used to determine the ellipticities. Equation 3 was fitted to each of our clusters via  $\chi^2$  minimization. The measured ellipticities for all clusters except NGC 121 should be considered as upper limits, because the data could be easily fit with a lower ellipticity and a similarly low  $\chi^2$ . Because we cannot measure the ellipticities at the tidal radii, the values presented here refer to the light distribution near  $r_h$ . The angular distributions are shown in Figure 10 and the results are summarized in Table 5.

#### 4. DISCUSSION

##### 4.1. Comparison of the core radii with previous studies

The only study of structural parameters of SMC star clusters based on space-based observations (HST/WFPC2) was presented by Mackey & Gilmore (2003b). They used imaging data of 10 populous star clusters. Four of these clusters are also included in the

present sample. The most recent ground-based study of structural parameters was published by Carvalho et al. (2008) and is based on data taken with the Danish 1.54 m telescope at the European Southern Observatory, La Silla, Chile. These authors studied surface photometry of 25 SMC star clusters, of which four overlap with our sample. Hill & Zaritsky (2006) used data from the Magellanic Clouds Photometric Survey (MCPS) (Zaritsky et al. 2002). Structure parameters were derived from fitting both King and EFF profiles for 204 star clusters. McLaughlin & van der Marel (2005) fitted both King and EFF models to star-count data for clusters in the SMC of which four overlap with the present sample. The observed profiles come from combining the ground-based photographic data from Mackey & Gilmore (2003b) with data from Kontizas et al. (1982) and Kontizas & Kontizas (1983). Earlier studies using number-density profiles were published by Kontizas et al. (1990) and are based on photographic plates obtained with the 1.2 m U.K. Schmidt Telescope in Australia. Five clusters of the present sample were also studied by Kontizas et al. (1990), but owing to the different resolution and depth of the shallower photographic plates we do not discuss these results here. As noted above, although often called the ‘core radius’, the King profile scale radius  $r_0$  is larger than the true core radius  $r_c$ , with the difference being large for lower central concentrations. This effect is illustrated in Fig. 7 where we plot the difference between  $r_0$  and  $r_c$  (derived from the EFF profile fits) against central concentration. We must therefore be careful to compare ‘like with like’, and we have thus compared our core radii from the EFF profile fits with literature data that also used EFF profile fits.

In Table 6 we compare the core radii from EFF profiles from surface-brightness profiles with the above mentioned previous studies. The EFF core radius of NGC 121 found in our study is  $\sim 1.4$  pc larger than the corresponding one published by Carvalho et al. (2008) and is  $\sim 0.75$  pc larger than the one found by Mackey & Gilmore (2003b) and McLaughlin & van der Marel (2005). The core radius of NGC 339 is  $\sim 0.9$  pc ( $\sim 11\%$ ) larger than the radius published by Carvalho et al. (2008) ( $1 \text{ pc} = 3.4''$ ), while the core radii of NGC 416 and Kron3 are in good agreement. The core radii of Kron3 and NGC 339 are  $\sim 0.6$  pc ( $\sim 10\%$ ) larger than the ones found by Mackey & Gilmore (2003b) while the core radius of NGC 416 agrees well with our value. The core radii of Kron3 and NGC 339 are in very good agreement with McLaughlin & van der Marel (2005), but the core radius of NGC 416 is  $\sim 0.5$  pc ( $\sim 18\%$ ) smaller. Comparing our result with Hill & Zaritsky (2006) we find that their core radii for NGC 339, NGC 416, and NGC 419 are all larger than the values of this study by about 0.5 pc, 0.4 pc, and 1.5 pc, respectively.

Comparing the half-light radii for NGC 121, Kron 3, and NGC 339 determined by estimating  $L_{tot}$  using surface-brightness data to those radii published by McLaughlin & van der Marel (2005), we find that their half-light radii of NGC 121, Kron 3, and NGC 339 are  $\sim 16\%$  (5.96 pc),  $\sim 27\%$  (10.54 pc), and  $\sim 26\%$  (12.65 pc) smaller than those found in this study. The remaining clusters of the present sample do either not overlap or

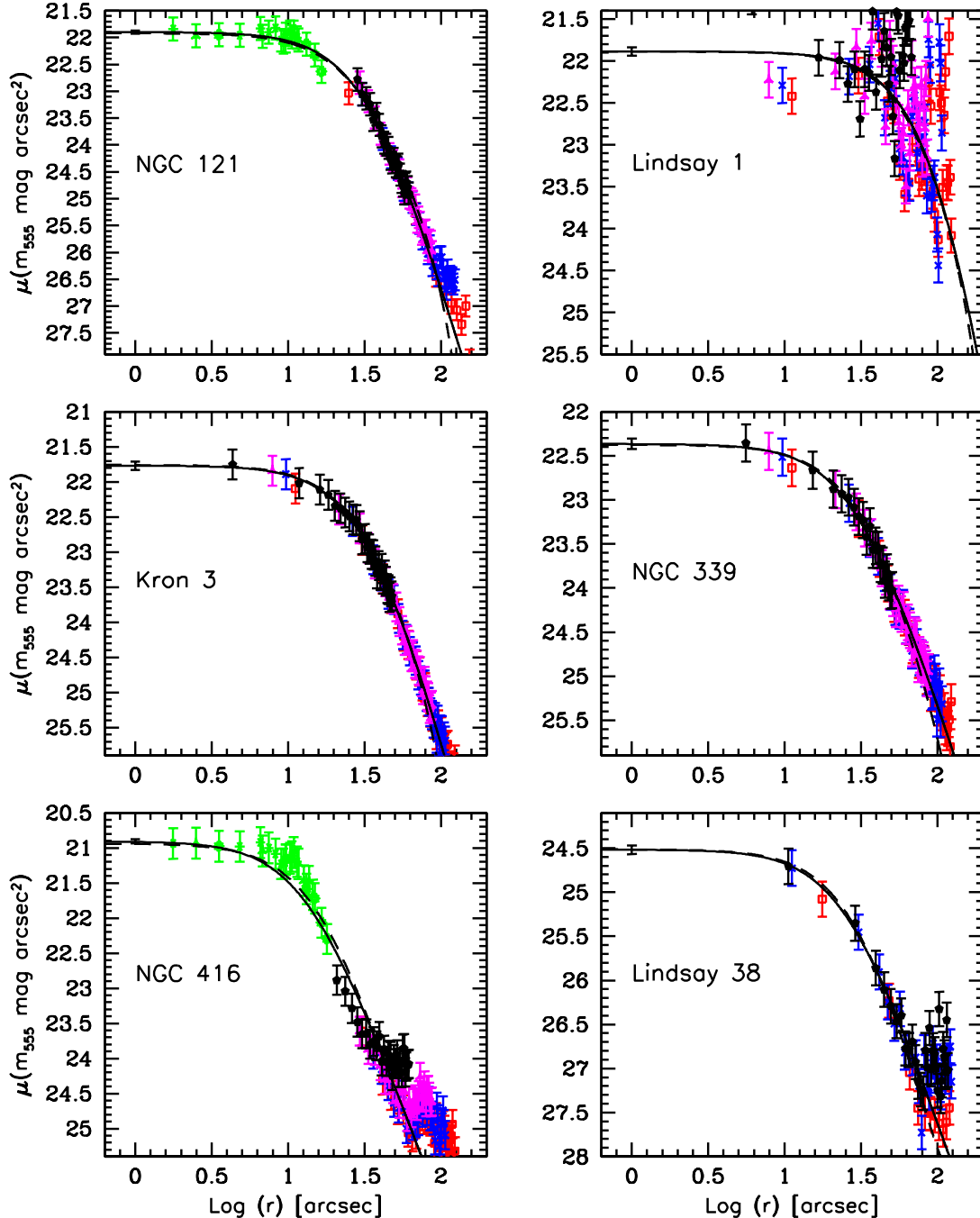


FIG. 8.— For this set of profiles all cluster stars brighter than the magnitude for which the completeness is 50% in the cluster central region and fainter than the MSTO were used. The applied method is the same as for the first set of EFF profiles shown in Fig. 5 and 6.

the half-light radii could not be calculated.

In the LMC, Mackey & Gilmore (2003a) found evidence for double or post-core-collapse (PCC) clusters in the surface brightness profiles among the oldest clusters, as well as in one globular cluster in the Fornax dwarf spheroidal galaxy (Mackey & Gilmore 2003c). A PCC cluster is characterized by an apparent power-law profile in its innermost region, which is different from a constant-density core as found in the EFF and King profiles. No evidence of this kind of clusters was found for SMC clusters (Mackey & Gilmore 2003b) or in our study.

One additional uncertainty in the inter-comparisons of physical cluster core and tidal radii is the distance modulus. In previous studies a single distance modulus was assumed and applied to the calculations. However, the SMC may have a depth extent of up to 20 kpc (Mathewson et al. 1988; Hatzidimitriou et al. 1993; Crowl et al. 2001; Lah et al. 2005). With the exception of NGC 419, for which we used isochrone fitting, we determined the distance modulus for each cluster using the red clump magnitude (Glatt et al. 2008a). However, no correlation between core radius and distance

TABLE 5  
ELLIPTICITIES

Cluster	Distance from SMC center [kpc]	age Gyr	R arcmin	$\epsilon$	$\theta_p \pm 180$ degree	$\alpha$	$\sigma_b$ arcmin <sup>2</sup>
NGC 121	$8.76 \pm 1.1$	$10.5 \pm 0.5$	1.17	$0.27 \pm 0.06$	83	1.77	22.48
Lindsay 1	$13.28 \pm 1.0$	$7.5 \pm 0.5$	1.52	0.16	83	0.96	23.85
Kron 3	$7.19 \pm 1.1$	$6.5 \pm 0.5$	1.22	0.14	88	0.96	28.80
NGC 339	$0.73 \pm 2.0$	$6 \pm 0.5$	1.46	0.17	76	0.90	62.55
NGC 416	$3.94 \pm 1.4$	$6 \pm 0.8$	1.04	0.17	109	0.90	264.33
Lindsay 38	$6.27 \pm 1.3$	$6.5 \pm 0.5$	1.18	0.21	109	0.88	17.82
NGC 419	$10.83 \pm 1.6$	$1.2 - 1.6$	1.14	0.14	86	1.10	90.45
<i>Literature Sample</i>							
NGC 411	$11.1 \pm 1.3$	$1.2 \pm 0.2$	-	0.08	-	-	-
NGC 152	$5.58 \pm 1.3$	$1.4 \pm 0.2$	-	0.23	-	-	-
Kron 28	$14.78 \pm 1.3$	$2.1 \pm 0.5$	-	0.30	-	-	-
Kron 44	$4.37 \pm 1.3$	$3.1 \pm 0.8$	-	0.26	-	-	-
BS90	1.23	$4.3 \pm 0.1$	-	0.05	-	-	-

<sup>a</sup>The cluster 3d-distances from the SMC center were calculated in Paper I. R lists the radii within which all stars for the angular distribution calculation were considered. The ellipticities come from this paper and the literature values were adopted from Hill & Zaritsky (2006). All ellipticities determined in this study except the one for NGC 121 should be considered as upper limits. The ages are taken from Paper I, II and Alves & Sarajedini (1999); Crowl et al. (2001); Piatti et al. (2001); Sabbi et al. (2007).

TABLE 6  
COMPARISON OF  $r_c$  [PC] FROM EFF MODEL FITS TO LITERATURE DATA

Reference	NGC 121	Lindsay 1	Kron 3	NGC 339	NGC 416	Lindsay 38	NGC 419
This paper	$3.75 \pm 0.39$	$13.81 \pm 0.60$	$6.70 \pm 0.26$	$8.10 \pm 0.11$	$2.65 \pm 0.07$	$9.30 \pm 0.48$	$2.85 \pm 0.09$
Carvalho et al. (2008)	$2.39 \pm 0.01$	-	-	$7.23 \pm 0.71$	$2.30 \pm 0.01$	-	$2.93 \pm 0.01$
Hill & Zaritsky (2006)	-	-	-	8.62	3.05	-	4.04
McLaughlin & van der Marel (2005)	$3.05 \pm 0.10$	-	$6.92 \pm 0.26$	$7.98 \pm 0.45$	$3.13 \pm 0.10$	-	-
Mackey & Gilmore (2003b)	$3.02 \pm 0.10$	-	$6.07 \pm 0.18$	$7.05 \pm 0.30$	$2.84 \pm 0.10$	-	-

<sup>a</sup>The core radii of Mackey & Gilmore (2003b); McLaughlin & van der Marel (2005); Hill & Zaritsky (2006) have been converted to the distances found in Paper I.

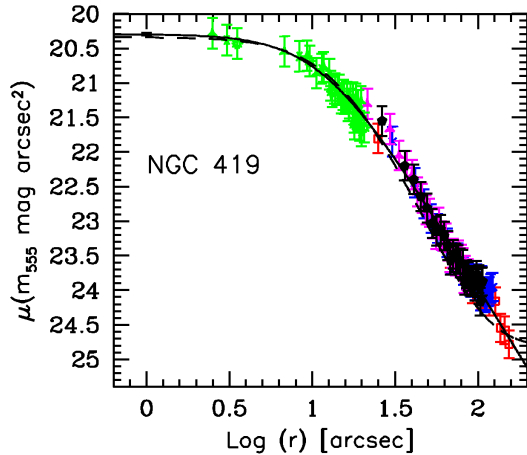


FIG. 9.— As for Fig. 8 but for NGC 419.

from the SMC center was found (Fig. 11).

#### 4.2. Age-radius relation

In the LMC, a trend for larger core radii with increasing age has been found (Mackey & Gilmore 2003a) and evidence for the same trend appears to be present in the SMC (Mackey & Gilmore 2003b). In their studies,

core radii of 10 SMC star clusters and 53 LMC clusters were determined using EFF profiles and compared to each other. The SMC clusters may have slightly larger core radii on average than the LMC clusters, but the authors claimed that this could be the result of uncertainties in both the SMC distance modulus (for all clusters a distance modulus of 18.9 was used) and the large depth extension of the SMC. The youngest SMC and LMC clusters all had compact cores, whereas older clusters showed a bifurcation with most clusters following a lower sequence and some clusters exhibiting increased core radii.

Combining our results and literature values (Tab. 7), we confirm the proposed relationship between cluster age and spread in core size in the SMC. In Figure 12 core radii from EFF profiles are shown. The trend of older clusters having a larger range in core radii than the younger population is clearly visible. The oldest star cluster, NGC 121, has a small core radius of  $3.75 \pm 0.39$  pc, while for the second oldest cluster, Lindsay 1, the core radius is rather large with  $13.81 \pm 0.60$  pc. One of our intermediate-age clusters has a radius larger than 10 pc (Lindsay 1). The intermediate-age cluster Kron 44 has the largest core radius of the literature sample ( $r_c = 11.18$  pc; Hill et al. 2006). Its age is  $3.1 \pm 0.8$  Gyr (Piatti et al. 2001). Star clusters younger than 1 Gyr have core radii smaller than 4 pc. Nevertheless, only Lindsay 1 and Kron 44 have

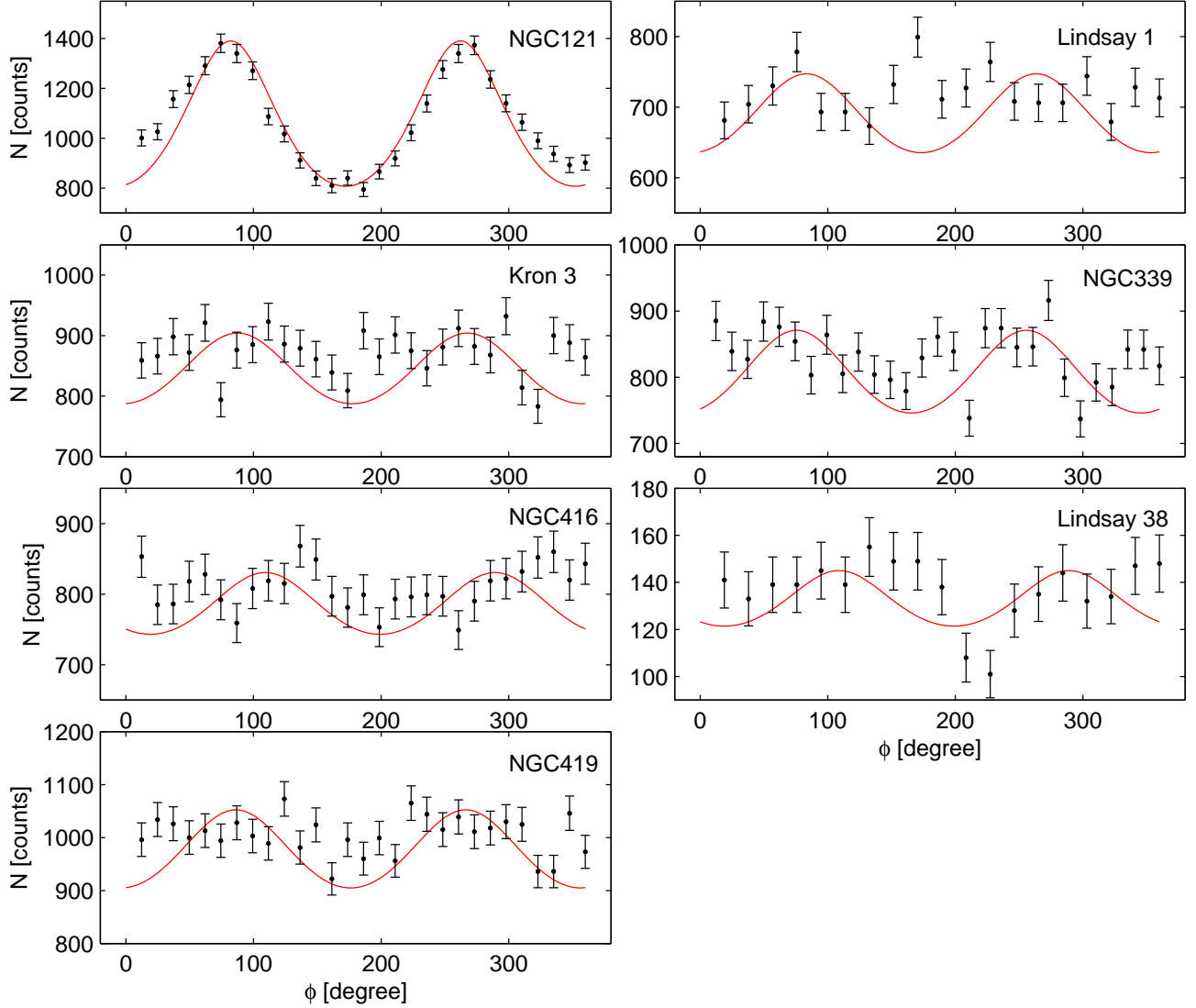


FIG. 10.— The angular distribution of member stars that lie entirely on the ACS images around the determined center of gravity. The solid red curves are the best fits of Eq.(3) of the text, indicating the ellipticity of the clusters. The measured ellipticities for all clusters except the one for NGC 121 should be considered as upper limits, because the data could be easily fit with a lower ellipticity and a similarly low  $\chi^2$ .

significantly larger core radii than the rest of the clusters considered here. The clusters NGC 361, NGC 152, Kron 28, Lindsay 11, Kron 3, NGC 339, and Lindsay 38 have radii between 5 and 8.5 pc, which is slightly larger on average than the core radii of the remaining 21 clusters, whose core radii are smaller than 5 pc. Figure 12 suggests that among the older clusters some objects seem to have experienced a significant change in  $r_c$ , while for others  $r_c$  remained almost unaltered.

For GCs, the concentration parameter  $c$  traditionally is around or even larger than 1, implying a compact isothermal central region and an extended tidally truncated outer region, while open clusters are more diffuse objects (e.g., Harris 1996; Binney & Merrifield 1998; Bonatto & Bica 2008). The oldest and only globular cluster in the SMC, NGC 121, has a concentration parameter of  $c = 1.034 \pm 0.12$ . For comparison, the Galac-

tic globular clusters 47 Tuc, NGC 288, and NGC 6909, all non-PCCs, have  $c = 2.04$ ,  $c = 0.98$ , and  $c = 0.76$  (Harris 1996). The youngest cluster in the present sample, NGC 419, with an age of 1.2-1.6 Gyr, has a globular cluster-like concentration parameter of  $c = 1.059 \pm 0.08$ . This is the case for all three profiles. In its CMD we see indications of a double or even multiple main sequence turnoffs (see Paper I), a feature seen also in the two LMC star clusters, NGC 1846 and NGC 1806, known to have a double main-sequence turn-off (Mackey et al. 2008, see also Mackey & Broby Nielson 2007).

Plotting mass versus core radius does not show any correlation for LMC and SMC star clusters (Mackey & Gilmore 2003a,b), and no significant difference between masses of young and old clusters was found. If only massive star clusters had large core radii one could argue that the younger low-mass clusters dispersed after a few Gyr, but at least in the LMC and SMC this does

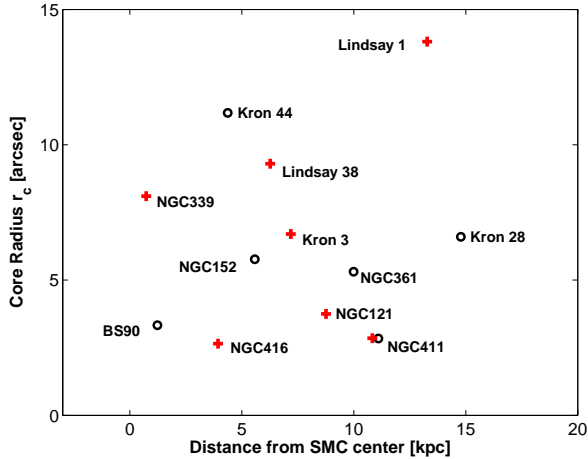


FIG. 11.— Core radii vs distance from the SMC center for the clusters in our sample (plus) and clusters for which reliable distances were found in the literature (circles). The distances were adopted from Paper I and Crowl et al. (2001). The core radii for NGC 152, NGC 361, and NGC 411 are taken from Mackey & Gilmore (2003b), while for Kron 28 and Kron 44 the values are taken from Hill & Zaritsky (2006).

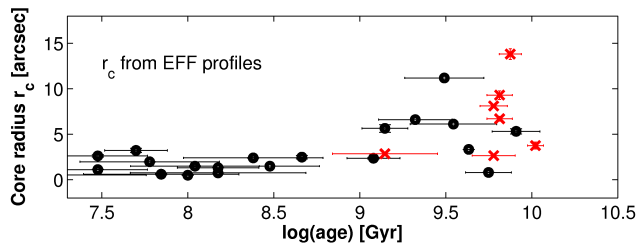


FIG. 12.— Age vs core radius  $r_c$  of our cluster sample (crosses) and additional sample found in the literature (circles). The adopted core radii and ages are listed in Table 7. Because the errors of the EFF core radii in both our and in the literature sample are very small, the errorbars are barely visible.

not seem to be the case. Since the age-radius correlation has been observed in the combined sample of SMC, LMC, Fornax, and Sagittarius star clusters, Mackey & Gilmore (2003c) emphasized the possibility of a universal physical process as the origin of this trend. While our results are consistent with this possibility, additional observations and theoretical studies are needed to establish if an internal process is at work.

#### 4.3. Cluster evolution

It is intriguing that LMC and SMC clusters seem to have experienced a similar structural evolution, even though the two galaxies show strong differences in various other aspects. The SMC contains only one old GC, NGC 121, which is 2-3 Gyr younger than the oldest GC in the LMC and MW (Paper II). The second oldest SMC star cluster, Lindsay 1, has an age of  $7.5 \pm 0.5$  Gyr, and since then compact populous star clusters have formed fairly continuously until the present day (e.g., Da Costa 2002; Glatt et al. 2008a). Furthermore, the intermediate-age clusters in the SMC appear to be capable of surviving for a Hubble time, due to their high mass and the structure of the SMC (no bulge or disk to be passed; Hunter et al. 2003; Lamers et al. 2005; Gieles

TABLE 7  
LITERATURE SAMPLE

Cluster	age Gyr	$r_{c, EFF}$ pc	References
NGC 176	$0.46 \pm 0.01$	$2.48 \pm 0.19$	1, 14
Kron 17	$0.30 \pm 0.10$	$1.49 \pm 0.01$	2, 15
NGC 241 + 242	$0.07 \pm 0.04$	$0.60 \pm 0.07$	3, 15
NGC 290	$0.03 \pm 0.01$	$1.11 \pm 0.03$	4, 15
Lindsay 48	$0.15 \pm 0.04$	$1.32 \pm 0.02$	1, 15
Kron 34	$0.24 \pm 0.12$	$2.39 \pm 0.04$	3, 15
NGC 330	$0.03 \pm 0.01$	$2.61 \pm 0.12$	5, 14
Lindsay 56	$0.006 \pm 0.01$	$0.51 \pm 0.01$	4, 15
NGC 346	$\sim 0.003$	$2.01 \pm 0.03$	6, 6
IC 1611	$0.11 \pm 0.05$	$1.49 \pm 0.06$	3, 15
IC 1612	$\sim 0.10$	$0.49 \pm 0.01$	7, 15
Lindsay 66	$0.15 \pm 0.10$	$0.74 \pm 0.01$	8, 15
NGC 361	$8.10 \pm 1.20$	$5.31 \pm 0.28$	9, 14
Kron 47	$\sim 0.007$	$1.74 \pm 0.15$	7, 15
IC 1624	$0.06 \pm 0.03$	$1.97 \pm 0.03$	3, 15
NGC 411	$1.20 \pm 0.20$	$2.84 \pm 0.11$	10, 14
NGC 458	$0.05 \pm 0.01$	$3.22 \pm 0.24$	1, 14
Lindsay 114	$5.60 \pm 0.50$	$0.80 \pm 0.02$	4, 4
NGC 152	$1.4 \pm 0.20$	$5.77 \pm 0.42$	11, 14
Kron 28	$2.1 \pm 0.50$	6.60	12, 15
Kron 44	$3.1 \pm 0.80$	11.18	12, 15
Lindsay 11	$3.5 \pm 1$	6.11	13, 15
BS90	$4.3 \pm 0.10$	3.33	6, 15

<sup>a</sup>The cluster ages we adopted from: (1) Hodge (1983), (2) Hodge & Flower (1987), (3) Elson & Fall (1985), (4) Ahumada et al. (2002), (5) Da Costa & Hatzidimitriou (1998), (6) Sabbi et al. (2007), (7) Chiosi et al. (2006), (8) Piatti et al. (2005), (9) Mighell et al. (1998), (10) Alves & Sarajedini (1999), (11) Crowl et al. (2001), (12) Piatti et al. (2001), (13) Mould et al. (1992), and the EFF core radii from: (14) Mackey & Gilmore (2003b) and (15) Carvalho et al. (2008).

et al. 2007). However, the SMC has a moderately dense "bar" and we do not know how its clusters orbit in the SMC.

In contrast to the SMC, the LMC had two main epochs of cluster formation (e.g., Bertelli 1992) and a well-known "age-gap" between  $\sim 4$ -9 Gyr (e.g., Holtzman et al. 1999; Johnson et al. 1999; Harris & Zaritsky 2001), in which no (surviving) star clusters have formed. Several GCs are found with coeval ages like the Galactic GCs and GCs in other dwarf galaxies (e.g., Olszewski et al. 1991; Olsen et al. 1998; Johnson et al. 1999; Grebel & Gallagher 2004). We know only of one LMC star cluster, ESO 121-SC03, that has an age of 8.3-9.8 Gyr (Mackey et al. 2006), which defines the lower limit of the old LMC star cluster age distribution.

In the SMC, Hill & Zaritsky (2006) found the distribution of cluster core sizes to be broader than in the MW, which they argue is due to a prevalence of surviving low-concentration clusters in the SMC. In her analysis of the LMC star clusters, Elson (1991) noted that for clusters of a given age, there appears to exist an upper limit for their core size. Moreover, this limit was found to increase with age, which was later confirmed by the analysis of Mackey & Gilmore (2003a). Young clusters are observed to have very compact cores of e.g.  $\sim 2.13$  pc (NGC 1711) and  $\sim 1.33$  pc (NGC 1805), whereas the cores of older clusters can reach extents of up to 13 pc.

N-body simulations of Goodwin & Bastian (2006) illustrate how the structural parameters of star clusters change with time. A major driver of these changes is the



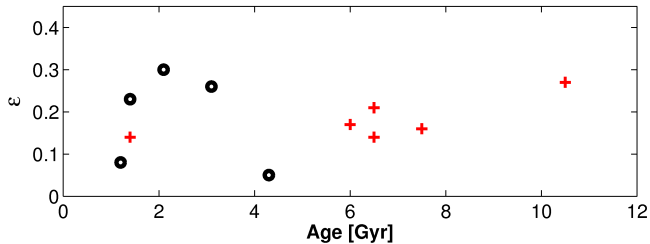


FIG. 13.— Age vs ellipticity showing the clusters from our sample (crosses) and five clusters from the literature (circles). The ellipticities for NGC 152, NGC 411, Kron 28, Kron 44, and BS90 are taken from Hill & Zaritsky (2006) and the ages from Alves & Sarajedini (1999); Crowl et al. (2001); Piatti et al. (2001); Sabbi et al. (2007). It seems that the younger clusters tend to be flatter than the older clusters, although NGC 121 is the oldest and the flattest cluster. The measured ellipticities in this study, except the one of NGC 121, should be considered as upper limits.

expulsion of gas, which was not converted into stars via star formation. The minimum local star formation efficiency to leave a bound massive star cluster is  $\sim 25\%$ , and higher efficiencies are possible (e.g., Parmentier & Fritze 2009). But even in efficient cases, a significant amount of unused gas remains. Kroupa & Boily (2002) suggested that populous star clusters expel their unused gas explosively due to the presence of numerous O stars during their early evolutionary stages. Goodwin & Bastian (2006) also suggested a rapid gas removal caused by stellar winds and supernovae during the first 20 Myr. As a consequence the young clusters may find themselves out of virial equilibrium; the stars have too large a velocity dispersion for the new, reduced gravitational potential. In order to re-stabilize, the cluster expands on a few crossing times scales of  $< 10$  Myr (see e.g., Sabbi et al. 2007). The most extreme core radii can be explained by external processes (e.g., for clusters that are not isolated), or by radically different stellar populations (mergers of clusters and effects from variable tidal fields, Mackey & Gilmore 2003a).

Various estimates of characteristic cluster disruption time-scales in different star cluster environments have been calculated (e.g., Gieles & Bastian 2008; Parmentier & de Grijs 2008). Many studies were based on a constant cluster formation rate (CFR) as a function of time. The poorly understood time-variable CFR of the LMC and SMC complicates such an analysis. Parmentier & de Grijs (2008) analyzed the cluster disruption time-scale in the LMC using Monte Carlo simulations. For younger clusters (age  $< 5$  Gyr), the general behavior of the CFR is recovered. It has been increasing steadily from about  $0.3$  clusters  $\text{Myr}^{-1}$  5 Gyr ago to a present rate of  $\sim 25$  clusters  $\text{Myr}^{-1}$ . For older clusters (age  $> 5$  Gyr), the CFR is very uncertain. It is possible that the CFR has increased steadily over a Hubble-time from  $\sim 1$  cluster  $\text{Gyr}^{-1}$  13 Gyr ago to its present value. For the SMC such studies have not been published, but the lack of very old SMC star clusters shows that the CFR of the LMC and SMC either varies significantly or that the CFR was rather constant but most clusters dissolved before reaching intermediate ages.

#### 4.4. Ellipticities

##### 4.4.1. Comparison with previous studies

None of the clusters in our sample exhibits a significant flattening except NGC 121 and Lindsay 38, the sparsest cluster in the present sample. Because the tidal radii of our clusters lie outside the ACS images, we have to assume that the ellipticities in the clusters' interiors are the same as at the tidal radii. For Lindsay 38, no ellipticity determination was found in the literature.

Measuring ellipticities is strongly dependent on the correct determination of the cluster center. Background and foreground determination, as well as stochastic effects influence the determination of isophotes. However, as much of the SMC is not crowded and at high Galactic latitude (e.g., Ratnatunga & Bahcall 1985), the effects of field star contamination should not be severe. Another explanation for the large SMC cluster ellipticities might be the influence of the local SMC field star background, the different measuring methods as well as the differing radii at which the ellipticities were measured. Some Galactic globular clusters have been found showing increasing ellipticities at larger distances from the cluster core (White & Shawl 1987). These might be the reasons for the differences between the values presented here and those found by Kontizas et al. (1990) and Hill & Zaritsky (2006). We have to emphasize that the determination of the ellipticity is quite uncertain, especially when it is fairly small as it is for most of the present clusters. The results of the the present study and the literature data are in good agreement (Table 8).

##### 4.4.2. Astrophysical Implications

The flattening distributions of star clusters in the SMC, LMC and the MW are known to be very different (e.g., Kontizas et al. 1989; Han & Ryden 1994; Goodwin 1997). SMC star clusters in their outer regions are typically much more flattened than those of the MW and even flatter than those in the LMC (Kontizas et al. 1990). In Figure 13 we show the relation of ellipticity versus age. No evident correlation can be seen. Unfortunately, not enough reliable distances have been measured to make an accurate statement about a possible dependence on galactocentric radius in the LMC and the SMC for a large sample of clusters. We extend our sample by adding five populous star clusters for which reliable distances, ages, and ellipticities have been determined elsewhere in the literature (see Table 5 for references). The younger clusters (age  $\lesssim 5$  Gyr) seem to be flatter (larger  $\epsilon$ ) than the older objects. In the MW, the flatter GCs are located close to the Galactic center, while for SMC such a correlation is not visible. Clusters lying behind the SMC center seem to be flatter than the ones lying in front. But we have to emphasize that the shown sample is very small and highly incomplete.

Like the SMC, the LMC does not show a relation between age and ellipticity, while clusters of all ages are significantly more elliptical than the Galactic GCs (Goodwin 1997). The Galactic GCs appear to modify their original structure and become less flattened at higher age. Han & Ryden (1994) argue that the difference between GC ellipticities in the LMC and the Milky Way are caused by the morphologies of the parent galaxies. They further showed that the GCs also vary in their shapes: LMC and SMC clusters are well-represented by triaxial spheroids, while Galactic GCs are oblate spheroids. Young LMC clusters appear to

TABLE 8  
COMPARISON OF THE ELLIPTICITIES

Reference	NGC 121	Lindsay 1	Kron 3	NGC 339	NGC 416	Lindsay 38	NGC 419
This paper	$0.27 \pm 0.06$	0.16	0.14	0.17	0.17	0.21	0.14
Hill & Zaritsky (2006)	-	-	-	0.17	0.11	-	0.09
Kontizas et al. (1990)	0.28	0.10	0.10	0.23	0.13	-	0.23
Geyer et al. (1983)	0.30	-	-	-	-	-	-

<sup>a</sup>The ellipticities by Kontizas et al. (1990) were measured at the inner-most parts. All ellipticities determined in this study except the one for NGC 121 should be considered as upper limits.

be highly flattened. Did the original structure of the older Galactic population get modified during their lifetime, and if yes, why did the old LMC and SMC cluster population remained unchanged? This may be explained with the different dynamical influence and therefore the varying strength of the tidal field of the parent galaxy (van den Bergh 2008). A strong tidal field will make the Galactic GCs more spherical during their orbits around the galaxy. The LMC and SMC have a totally different structure and no bulge or disk has to be passed (Hunter et al. 2003; Lamers et al. 2005; Gieles et al. 2007). The tidal field of the LMC and the SMC might not be strong enough to modify the shape of their clusters significantly, which might be the reason for their flat shapes. This point merits further exploration, e.g. via massive star cluster shape studies in nearby starburst and normal galaxies.

## 5. SUMMARY

We derive structural parameters for the seven SMC star clusters NGC 121, Lindsay 1, Kron 3, NGC 339, NGC 416, Lindsay 38, and NGC 419 based on stellar number density and surface brightness profiles and HST/ACS stellar photometry. We used King and EFF models to determine core radii, half-light radii, tidal radii, concentration parameters, and ellipticities of the star clusters. Half-light radii could only be estimated because the tidal radii lie outside the field of view of the ACS images.

Although our sample of SMC clusters is highly incomplete even after adding literature values, we confirm the result of Mackey & Gilmore (2003b) who found an increased scatter in core radii for older clusters (age > 1 Gyr) in dwarf galaxies. In the LMC this trend is more apparent (Mackey & Gilmore 2003a), perhaps a result of the LMC containing a much larger number of star clusters than the SMC.

We find intermediate age star clusters in the SMC to have larger half light radii and smaller concentration parameters than typical Galactic globular clusters of similar mass (e.g., Djorgovski & Meylan 1994). Indeed some of the clusters in this study could be classified as “faint fuzzies” based on their sizes and luminosities (Sharina et al. 2005). Thus these SMC clusters add to the trend for low density galaxies to contain older survivor star clusters with relatively high masses with a wide range of central densities extending from the dense globular cluster regime to quite low values.

The cluster formation history of the LMC also appears to be quite different from that of the SMC. The similar cluster structural patterns in the two galaxies is therefore intriguing. In the MW, many of the oldest clus-

ters experienced modifications of their original structure during their lifetimes, and many of the oldest halo clusters have developed cores, probably due to internal processes. One possible additional reason for the differences in the evolution of cluster structures between MW and SMC might be the morphology of the host galaxies. Low central concentration clusters can more easily survive in the SMC and LMC, while in the MW clusters have to pass the Galactic disk or bulge while orbiting the Galaxy. The lack of correlation between core radius and distance from the SMC center and the low density of the SMC both suggests that the cluster structures are little disturbed by external effects within these galaxies and primarily are driven by internal dynamical evolution (e.g., McLaughlin & van der Marel 2005).

Our data also show that the inner regions of intermediate-age clusters in this sample have rather spherical shapes, while in their outer zones and the oldest cluster, NGC 121, have higher ellipticities. Previous studies found higher ellipticities for the intermediate-age clusters at larger radii. We find no correlation between outer ellipticity and age, or outer ellipticity and distance from the SMC center, where we can take advantage of the 3-D information on the SMC cluster distribution from Paper I. Consistent with our conclusion regarding structures, the shapes of SMC clusters could remain elliptical if they experience little externally driven dynamical modification during their lifetimes.

This study indicates that the properties of the rich SMC star clusters are largely determined by internal processes. These objects thus can provide powerful tests for models of the intrinsic dynamical evolution of star clusters, while also serving as evolutionary markers for the SMC. Combinations of data from the MW and its satellites will continue to illuminate the actions of the internal and external astrophysical processes that shape star clusters.

We would like to thank an anonymous referee for his or her useful comments. We gratefully acknowledge support by the Swiss National Science Foundation through grant number 200020-105260 and 200020-113697. Support for the US component of this program GO-10396 was provided by NASA through a grant from the Space Telescope Science Institute, which is operated by the Association of Universities for Research in Astronomy, Inc., under NASA contract NAS 5-26555. Gisella Clementini and Monica Tosi have been partially supported by PRIN-MIUR-2004 and PRIN-INAF-2005. Andreas Koch acknowledges support by an STFC postdoctoral fellowship and Jay Gallagher also obtained helpful additional sup-

port from the University of Wisconsin Graduate School and from the Heidelberg Graduate School of Fundamental Physics within the framework of the Excellence Initia-

tive by the German Research Foundation (DFG) through grant number GSC 129/1.

## REFERENCES

- Ahumada, A. V., Clariá, J. J., Bica, E., & Dutra, C. M. 2002, *A&A*, 393, 855
- Alves, D. R., & Sarajedini, A. 1999, *ApJ*, 511, 225
- Bertelli, G., Mateo, M., Chiosi, C., & Bressan, A. 1992, *ApJ*, 388, 400
- Bertin, E., & Arnouts, S. 1996, *A&AS*, 117, 393
- Bica, E., Bonatto, C., Barbuy, B., & Ortolani, S. 2006, *A&A*, 450, 105
- Binney, J., & Merrifield, M. 1998, *Galactic astronomy*, Princeton, NJ : Princeton University Press, 1998. (Princeton series in astrophysics) QB8
- Bonatto, C., & Bica, E. 2008, *A&A*, 479, 741
- Carvalho, L., Saurin, T., Bica, E., Bonatto, C., & Schmidt, A. 2008, *A&A*, 485, 71
- Chiosi, E., Vallenari, A., Held, E. V., Rizzi, L., & Moretti, A. 2006, *A&A*, 452, 179
- Crowl, H. H., Sarajedini, A., Piatti, A. E., Geisler, D., Bica, E., Clariá, J. J., & Santos, J. F. C., Jr. 2001, *AJ*, 122, 220
- Da Costa, G. S. & Hatzidimitriou, D. 1998, *AJ*, 115, 1934
- Da Costa, G. S. 2002, in *IAU Symp. 207, Extragalactic Star Clusters*, ed. D. Geisler, E. K. Grebel, & D. Minniti (San Francisco: ASP), 83
- Dieball, A., Müller, H., & Grebel, E. K. 2002, *A&A*, 391, 547
- Djorgovski, S., & Meylan, G. 1994, *AJ*, 108, 1292
- Dotter, A., Chaboyer, B., Jevremović, D., Baron, E., Ferguson, J. W., Sarajedini, A., & Anderson, J. 2007, *AJ*, 134, 376
- Frenk, C. S., & Fall, S. M. 1982, *MNRAS*, 199, 565
- Elson, R. A. W., & Fall, S. M. 1985, *ApJ*, 299, 211
- Elson, R. A. W. 1991, *ApJS*, 76, 185
- Elson, R. A. W., Fall, S. M., & Freeman, K. C. 1987, *ApJ*, 323, 54
- Geyer, E. H., Nelles, B., & Hopp, U. 1983, *A&A*, 125, 359
- Glatt, K., et al. 2008a, *AJ*, 136, 1703
- Glatt, K., et al. 2008b, *AJ*, 135, 1106
- Gieles, M., & Bastian, N. 2008, *A&A*, 482, 165
- Gieles, M., Lamers, H. J. G. L. M., & Portegies Zwart, S. F. 2007, *ApJ*, 668, 268
- Gilmore, G., Wilkinson, M. I., Wyse, R. F. G., Kleyna, J. T., Koch, A., Evans, N. W., & Grebel, E. K. 2007, *ApJ*, 663, 948
- Girardi, L., Bressan, A., Bertelli, G., & Chiosi, C. 2000, *A&AS*, 141, 371
- Girardi, L., et al. 2008, *PASP*, 120, 583
- Gnedin, O. Y., & Ostriker, J. P. 1997, *ApJ*, 474, 223
- Goodwin, S. P., & Bastian, N. 2006, *MNRAS*, 373, 752
- Goodwin, S. P. 1997, *MNRAS*, 286, L39
- Grebel, E. K., & Gallagher, J. S., III 2004, *ApJ*, 610, L89
- Han, C., & Ryden, B. S. 1994, *ApJ*, 433, 80
- Harris, J., & Zaritsky, D. 2001, *ApJS*, 136, 25
- Harris, W. E. 1996, *AJ*, 112, 1487
- Hatzidimitriou, D., Cannon, R. D., & Hawkins, M. R. S. 1993, *MNRAS*, 261, 873
- Hill, A., & Zaritsky, D. 2006, *AJ*, 131, 414
- Hodge, P. W. 1983, *ApJ*, 264, 470
- Hodge, P., & Flower, P. 1987, *PASP*, 99, 734
- Holtzman, J. A. 1999, *AJ*, 118, 2262
- Hunter, D. A., Elmegreen, B. G., Dupuy, T. J., & Mortonson, M. 2003, *AJ*, 126, 1836
- Johnson, J. A. Bolte, M., Stetson, P. B., Hesser, J. E., & Somerville, R. S. 1999, *ApJ*, 527, 199
- King, I. 1962, *AJ*, 67, 471
- Koch, A., Grebel, E. K., Odenkirchen, M., Martínez-Delgado, D., & Caldwell, J. A. R. 2004, *AJ*, 128, 2274
- Koch, A., Wilkinson, M. I., Kleyna, J. T., Gilmore, G. F., Grebel, E. K., Mackey, A. D., Evans, N. W., & Wyse, R. F. G. 2007, *ApJ*, 657, 241
- Koekemoer, A. M., Fruchter, A. S., Hook, R. N., & Hack, W. 2002, in *Hubble after the Installation of the ACS and the NICMOS Cooling System*, ed. S. Arribas, A. Koekemoer & B. Whitmore (Baltimore: STScI), 337
- Kontizas, M., Danezis, E., & Kontizas, E. 1982, *A&AS*, 49, 1
- Kontizas, E., & Kontizas, M. 1983, *A&AS*, 52, 143
- Kontizas, M., Theodossiou, E., & Kontizas, E. 1986, *A&AS*, 65, 207
- Kontizas, E., Kontizas, M., Sedmak, G., & Smareglia, R. 1989, *AJ*, 98, 590
- Kontizas, E., Kontizas, M., Sedmak, G., Smareglia, R., & Dapergolas, A. 1990, *AJ*, 100, 425
- Kroupa, P., & Boily, C. M. 2002, *MNRAS*, 336, 1188
- Lah, P., Kiss, L. L., & Bedding, T. R. 2005, *MNRAS*, 359, L42
- Lamers, H. J. G. L. M., Gieles, M., & Portegies Zwart, S. F. 2005, *A&A*, 429, 173
- Mackey, A. D., & Gilmore, G. F. 2003a, *MNRAS*, 338, 85
- Mackey, A. D., & Gilmore, G. F. 2003b, *MNRAS*, 338, 120
- Mackey, A. D., & Gilmore, G. F. 2003c, *MNRAS*, 340, 175
- Mackey, A. D., Payne, M. J., & Gilmore, G. F. 2006, *MNRAS*, 369, 921
- Mackey, A. D., & Broby Nielsen, P. 2007, *MNRAS*, 379, 151
- Mackey, A. D., Broby Nielsen, P., Ferguson, A. M. N., & Richardson, J. C. 2008, *ApJ*, 681, L17
- Mathewson, D. S., Ford, V. L., & Visvanathan, N. 1988, *ApJ*, 333, 617
- McLaughlin, D. E., Harris, W. E., & Hanes, D. A. 1994, *ApJ*, 422, 486
- McLaughlin, D. E., Secker, J., Harris, W. E., & Geisler, D. 1995, *AJ*, 109, 1033
- McLaughlin, D. E., & van der Marel, R. P. 2005, *ApJS*, 161, 304
- Mighell, K. J., Sarajedini, A., & French, R. S. 1998, *AJ*, 116, 2395
- Mould, J. R., Jensen, J. B., & Da Costa, G. S. 1992, *ApJS*, 82, 489
- O'Connell, R. W., Gallagher, J. S., III, & Hunter, D. A. 1994, *ApJ*, 433, 65
- Olsen, K. A. G., Hodge, P. W., Mateo, M., Olszewski, E. W., Schommer, R. A., Suntzeff, N. B., & Walker, A. R. 1998, *MNRAS*, 300, 665
- Olszewski, E. W., Schommer, R. A., Suntzeff, N. B., & Harris, H. C. 1991, *AJ*, 101, 515
- Parmentier, G., & de Grijs, R. 2008, *MNRAS*, 383, 1103
- Parmentier, G., & Fritze, U. 2009, *ApJ*, 690, 1112
- Piatti, A. E., Santos, J. F. C., Clariá, J. J., Bica, E., Sarajedini, A., & Geisler, D. 2001, *MNRAS*, 325, 792
- Piatti, A. E., Santos, J. F. C., Jr., Clariá, J. J., Bica, E., Ahumada, A. V., & Parisi, M. C. 2005, *A&A*, 440, 111
- Plummer, H. C. 1911, *MNRAS*, 71, 460
- Ratnatunga, K. U., & Bahcall, J. N. 1985, *ApJS*, 59, 63
- Sabbi, E., et al. 2007, *AJ*, 133, 44
- Sharina, M. E., Puzia, T. H., & Makarov, D. I. 2005, *A&A*, 442, 85
- Sirianni, M. 2005, *PASP*, 117, 1049
- Storm, J., Carney, B. W., Gieren, W. P., Fouqué, P., Latham, D. W., & Fry, A. M. 2004, *A&A*, 415, 531
- Trager, S. C., King, I. R., & Djorgovski, S. 1995, *AJ*, 109, 218
- van den Bergh, S. 2008, *AJ*, 135, 1731
- White, R. E., & Shawl, S. J. 1987, *ApJ*, 317, 246
- Zaritsky, D., Harris, J., Thompson, I. B., Grebel, E. K., & Massey, P. 2002, *AJ*, 123, 855
- Zinn, R., & West, M. J. 1984, *ApJS*, 55, 45



